

**MEAN-FIELD APPROACH TO SUPERDEFORMED  
HIGH-SPIN STATES  
IN  $^{40}\text{Ca}$  AND NEUTRON-RICH  $^{50}\text{S}$  REGIONS**

T. INAKURA, M. YAMAGAMI, AND K. MATSUYANAGI

*Department of Physics, Graduate School of Science,  
Kyoto University, Kitashirakawa, Kyoto 606-8502, Japan*

S. MIZUTORI

*Department of Human Science, Kansai Women's College,  
Kashiwara City, Osaka 582-0026, Japan*

With the use of the symmetry-unrestricted cranked SHF method in the 3D coordinate-mesh representation, a systematic search for the SD and HD rotational bands in the  $N=Z$  nuclei from  $^{32}\text{S}$  to  $^{48}\text{Cr}$  has been done, and SD and HD solutions have been found in  $^{32}\text{S}$ ,  $^{36}\text{Ar}$ ,  $^{40}\text{Ca}$ ,  $^{44}\text{Ti}$ , and in  $^{36}\text{Ar}$ ,  $^{40}\text{Ca}$ ,  $^{44}\text{Ti}$ ,  $^{48}\text{Cr}$ , respectively. The SD band in  $^{40}\text{Ca}$  is found to be extremely soft against both the axially symmetric ( $Y_{30}$ ) and asymmetric ( $Y_{31}$ ) octupole deformations. Possible presence of SD states in neutron-rich sulfur isotopes from  $^{46}\text{S}$  to  $^{52}\text{S}$  has also been investigated, and deformation properties of neutron skins both in the ground and SD states are discussed.

## 1. Introduction

Quite recently, superdeformed(SD) rotational bands have been discovered in  $^{36}\text{Ar}$ ,  $^{40}\text{Ca}$ , and  $^{44}\text{Ti}$ .<sup>1,2,3</sup> One of the important new features of them is that they are built on excited  $0^+$  states and observed up to high spin, in contrast to the SD bands in heavier mass regions where low-spin portions of them are unknown in almost all cases. In this talk, we shall first report results of the symmetry-unrestricted, cranked Skyrme-Hartree-Fock (SHF) calculations for these SD bands. The calculation has been carried out with the use of the fully three-dimensional (3D), Cartesian coordinate-mesh representation without imposing any symmetry restriction.<sup>4,5,6</sup> The computational algorithm is basically the same as in the standard one<sup>7</sup> except that the symmetry restrictions are removed. For comparison sake, we also carry out the standard symmetry-restricted calculations imposing reflection symmetries about the  $(x, y)$ -,  $(y, z)$ - and  $(z, x)$ -planes. By com-

paring these results, we can clearly identify effects of reflection symmetry breaking in the mean field.

We shall next present results of the cranked SHF calculation for SD bands in the neutron-rich sulfur isotopes near the neutron drip line. These nuclei are expected to constitute a new “SD doubly closed” region associated with the SD magic numbers,  $Z = 16$  for protons and  $N \simeq 30$ -32 for neutrons. An interesting theoretical subject for the SD bands in these neutron-rich region is to understand deformation properties of neutron skins. We shall discuss on this point.

## 2. $^{40}\text{Ca}$ region

Figure 1 shows deformation energy curves evaluated by means of the constrained HF procedure. Solid lines with and without filled circles in these figures represent results of unrestricted and restricted calculations, respectively. In both cases, we obtain local minima corresponding to the SD states for  $^{32}\text{S}$ ,  $^{36}\text{Ar}$ ,  $^{40}\text{Ca}$  and  $^{44}\text{Ti}$  in the region  $0.4 \leq \beta_2 \leq 0.8$ . (The local minimum in  $^{44}\text{Ti}$  is triaxial so that it is not clearly seen the  $\gamma = 0$  section.) The local minima in  $^{32}\text{S}$  and  $^{36}\text{Ar}$  involve four particles in the  $fp$  shell, while those in  $^{40}\text{Ca}$  and  $^{44}\text{Ti}$  involve eight particles. In addition to these SD minima, we also obtain local minima in the region  $\beta_2 \geq 0.8$  for  $^{40}\text{Ca}$ ,  $^{44}\text{Ti}$  and  $^{48}\text{Cr}$ . These minima involve additional four particles in the single-particle levels that reduce to the  $g_{9/2}$  levels in the spherical limit. Somewhat loosely we call these local minima “hyperdeformed (HD).” The HD solution in  $^{40}\text{Ca}$  corresponds to the 12p-12h configuration.

We notice in this figure that the crossings between configurations involving different numbers of particles in the  $fp$  shell are sharp in the restricted calculations, while we always obtain smooth configuration rearrangements in the unrestricted calculations. The reason for this different behavior between the unrestricted and restricted calculations is rather easy to understand: When the parity symmetry is imposed, there is no way, within the mean-field approximation, to mix configurations having different number of particles in the  $fp$  shell. In contrast, as illustrated in Fig. 2, smooth crossover between these different configurations is possible via mixing between positive- and negative-parity single-particle levels, when such a symmetry restriction is removed. Octupole deformation parameters  $\beta_3$  are plotted as functions of  $\beta_2$  in the lower portion of Fig. 3 for the case of  $^{40}\text{Ca}$ . We see that values of  $\beta_3$  are zero near the local minima, but rise in the crossing region. This means that the configuration rearrangements

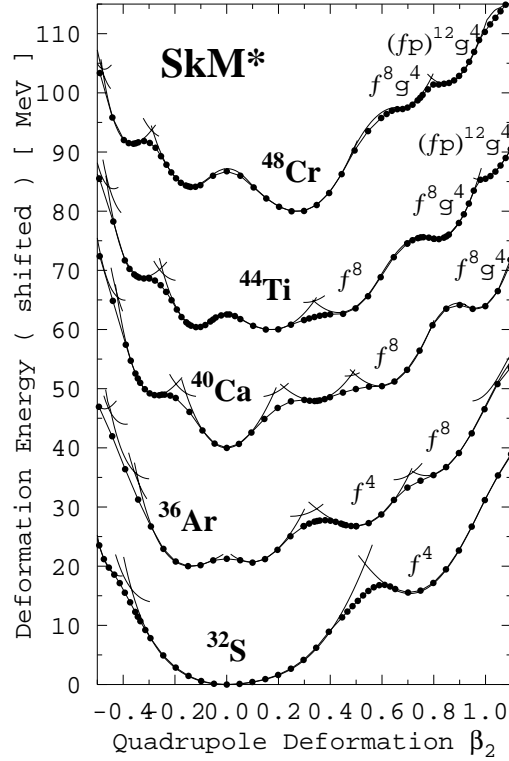


Figure 1. Deformation energy curves as functions of the quadrupole deformation  $\beta_2$  calculated at  $I = 0$  by means of the constrained SHF procedure with the SkM\* interaction. The axial-asymmetry parameter  $\gamma$  is constrained to be zero. The curves for different nuclei are shifted by 20 MeV in order to facilitate the comparison. Solid lines with and without filled circles represent the results obtained by the unrestricted and restricted versions, respectively (see the text). The notations  $f^n g^m$  and  $(fp)^n g^m$  indicate the configurations in which the  $f_{7/2}$  shell ( $fp$  shell) and the  $g_{9/2}$  shell are respectively occupied by  $n$  and  $m$  nucleons.

in fact take place through paths in the deformation space that break the reflection symmetry.

Excitation energies of the SD and HD bands in  $^{40}\text{Ca}$  calculated by using different versions (SIII, SkM\*, SLy4) of the Skyrme interaction are compared with the experimental data<sup>2</sup> in the left-hand portion of Fig. 4. The SD band is slightly triaxial with  $\gamma = 6^\circ\text{-}9^\circ(8^\circ\text{-}9^\circ)$  and it terminates at  $I \simeq 24$  for the SIII (SkM\*) interaction. (In the case of  $^{44}\text{Ti}$ , the shape is more triaxial with  $\gamma = 18^\circ\text{-}25^\circ$  and  $13^\circ\text{-}19^\circ$ , and the SD band terminates at  $I \simeq 12$  and 16 for the SIII and SkM\* interactions, respectively.<sup>6</sup>)

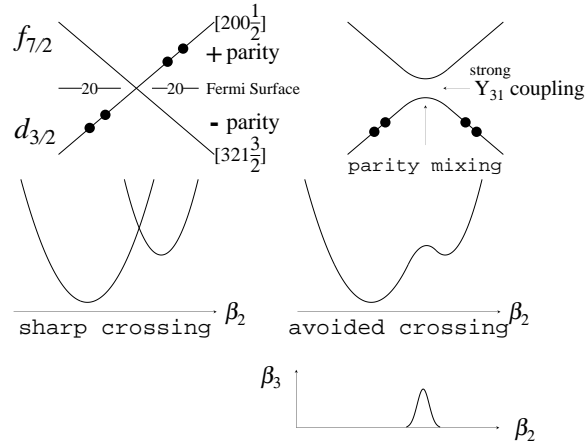


Figure 2. Level crossing between single-particle levels having opposite parities. Configuration rearrangement can take place by breaking the reflection symmetry in the mean field. The  $r^3 Y_{31}$  matrix element between levels with the asymptotic quantum numbers  $[321 \frac{3}{2}]$  and  $[200 \frac{1}{2}]$  is large, and significantly contributes to the tendency toward the non-axial  $Y_{31}$  octupole deformation discussed in the text.

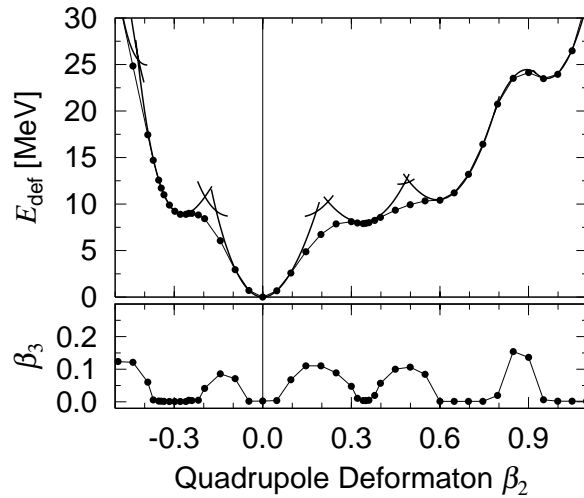


Figure 3. The upper part: Deformation energy curve for  $^{40}\text{Ca}$  (same as in Fig. 1). The lower part: Octupole deformation  $\beta_3$  obtained by the unrestricted SHF calculation with SkM\*, plotted as a function of  $\beta_2$ .

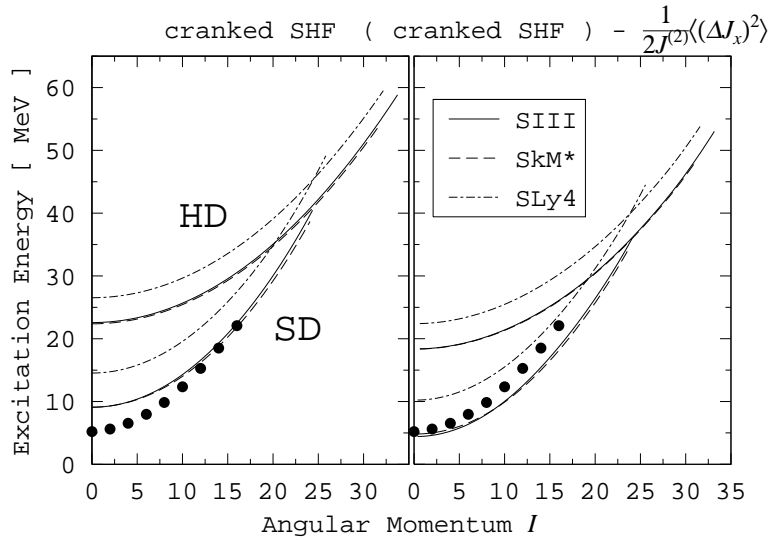


Figure 4. Comparison between the excitation energies of the SD and HD bands in  $^{40}\text{Ca}$ , calculated by using different versions of the Skyrme interaction and the experimental data (filled circles). Solid, dashed and dashed-dotted lines indicate the results with the SIII, SkM\* and SLy4 interactions, respectively. Results with and without including the zero-point rotational energy correction are shown in the right- and left-hand sides, respectively.

One may notice that the excitation energy of the SD band-head state is overestimated. We have evaluated the zero-point rotational energy correction,  $\frac{1}{2J^{(2)}}\langle(\Delta\hat{J}_x)^2\rangle$ , as a function of the rotational frequency  $\omega_{\text{rot}}$ . Here,  $\Delta\hat{J}_x = \hat{J}_x - \langle\hat{J}_x\rangle$  and  $J^{(2)}$  denotes the dynamical moment of inertia defined by  $J^{(2)} = dI/d\omega_{\text{rot}}$ . Excitation energies including this correction are shown in the right-hand portion of Fig. 4. We see that the calculated excitation energies are significantly improved by including this correction.

Let us examine stabilities of the SD local minimum in  $^{40}\text{Ca}$  against octupole deformations. Figure 5 shows deformation energy curves as functions of the octupole deformation parameters  $\beta_{3m}$  ( $|m| = 0, 1, 2, 3$ ) about the SD minimum. We immediately notice that the SD state is extremely soft with respect to the  $\beta_{30}$  and  $\beta_{31}$  deformations.

Quite recently, Imagawa and Hashimoto have carried out a selfconsistent RPA calculation in the 3D Cartesian-mesh representation on the basis of the SHF mean field, and they have obtained, for the SIII (SkM\*) interaction, a strongly collective octupole vibrational mode with  $K^\pi = 1^-$  at about

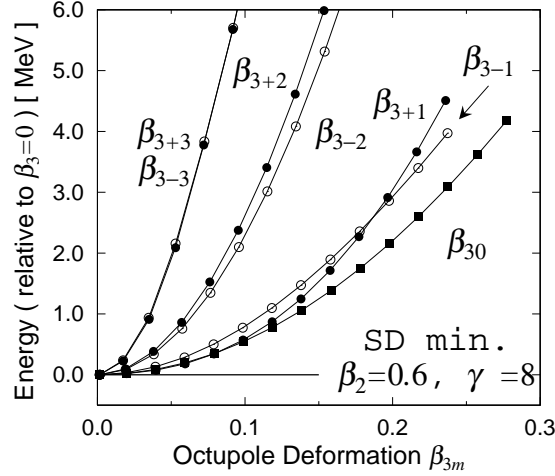


Figure 5. Deformation energy curves (measured from the energy at  $\beta_3 = 0$ ) as functions of the octupole deformation parameters  $\beta_{3m}$  ( $|m| = 0, 1, 2, 3$ ), calculated for  $^{40}\text{Ca}$  by means of the constrained HF procedure with SkM\*. The quadrupole deformation parameters are fixed at  $\beta_2 = 0.6$  and  $\gamma = 8^\circ$ . One of the  $\beta_{3m}$  ( $|m| = 0, 1, 2, 3$ ) is varied while the other  $\beta_{3m}$ 's are fixed to zero.

1.1 (0.6) MeV excitation from the SD band head.<sup>8</sup> Thus, it is extremely interesting to search for negative-parity rotational bands associated with the non-axial  $K^\pi = 1^-$  octupole vibrational modes built on the SD yrast band.

### 3. $^{50}\text{S}$ region

Figure 6 shows deformation energy curves for neutron-rich sulfur isotopes from  $^{46}\text{S}$  to  $^{52}\text{S}$ , which indicates that the SD local minima is deepest at  $^{50}\text{S}$ . As shown in Fig. 7, this result is common for the SHF calculations with the use of SIII, SkM\* and SLy4 interactions. Thus, the neutron SD shell structure seems to be slightly modified from that known in the Zn region with  $N \simeq Z$ , where  $N \simeq 30-32$  are the SD magic numbers.

Figures 8 and 9 show the neutron and proton density profiles for the ground and the SD states, respectively. We see that deformed neutron skins are present in both cases. These calculations are done with use of a small mesh size of 0.25 fm. In order to examine deformation properties of these neutron skins in more detail, we have made a least square fitting to the density distribution along each principal axis direction with the Woods-Saxon

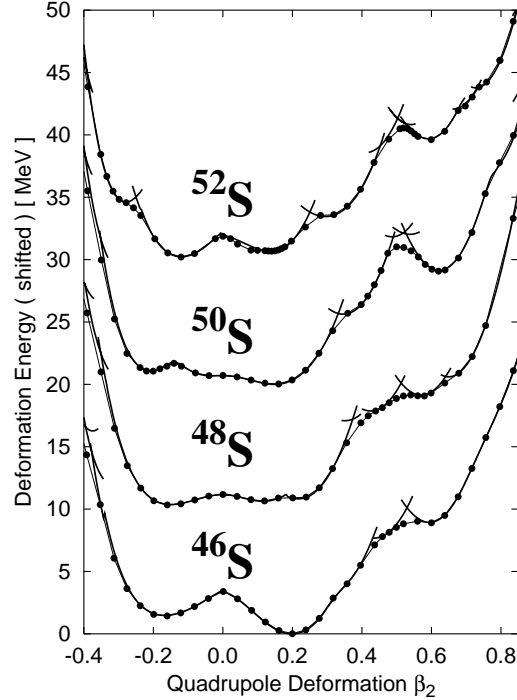


Figure 6. Deformation energy curves as functions of  $\beta_2$  calculated at  $I = 0$  by means of the constrained SHF procedure with the SLy4 interaction. The axial-asymmetry parameter  $\gamma$  is constrained to be zero. The curves for different nuclei are shifted by 10 MeV to facilitate the comparison. Solid lines with and without filled circles represent the results obtained by the unrestricted and restricted versions, respectively. The notations  $f^n g^m$  indicate the configurations in which the  $f_{7/2}$  shell and the  $g_{9/2}$  shell are respectively occupied by  $n$  and  $m$  nucleons.

function. The half-density radii and the diffuseness parameters extracted in this way for the SD state are listed in Table 1. We see that the neutron skin is formed mainly due to the difference in the diffuseness between protons and neutrons (rather than the difference in the half-density radius). It is interesting to note that the proton diffuseness parameter along the major axis is significantly smaller than that along the minor axis.

The presence of the deformed neutron skins may be detected through excitation spectra of these nuclei. Thus, search for soft  $K^\pi = 0^-$  and  $1^-$  (dipole + octupole) vibrational modes in unstable nuclei with deformed neutron skins seems especially interesting. Note that octupole modes will be mixed with dipole modes in deformed nuclei. For studying these modes,

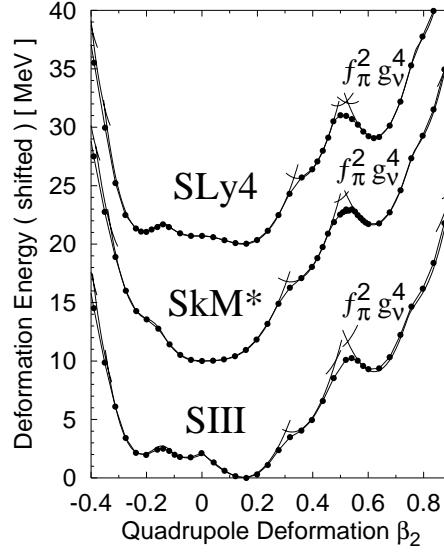


Figure 7. Comparison of deformation energy curves for  $^{50}\text{S}$  obtained by using different versions of the Skyrme interaction. The curves for different versions are shifted by 10 MeV.

Table 1. Root-mean square radii ( $R_{\text{rms}}$ ), quadrupole deformation parameters ( $\beta_2$ ), half-density radii for the major and minor axes ( $R_{1/2}^z$ ,  $R_{1/2}^x$ ), surface diffuseness parameters along the major and minor axes ( $a^z$ ,  $a^x$ ), evaluated by the SHF method with SLy4 for the SD state in  $^{50}\text{S}$ . The proton and neutron contributions are separately shown together with their differences.

SD	$R_{\text{rms}}$	$\beta_2$	$R_{1/2}^z$	$R_{1/2}^x$	$a^z$	$a^x$
neutrons	4.15	0.59	5.65	3.09	0.72	0.61
protons	3.75	0.70	5.76	2.77	0.38	0.47
differences	0.41	-0.11	-0.12	0.32	0.34	0.14

we need to develop the SHF-Bogoliubov + quasiparticle RPA approach such that we can take into account deformation, pairing, and continuum effects simultaneously. We can further envisage to go beyond the quasiparticle RPA by means of the selfconsistent collective coordinate method.<sup>9</sup>

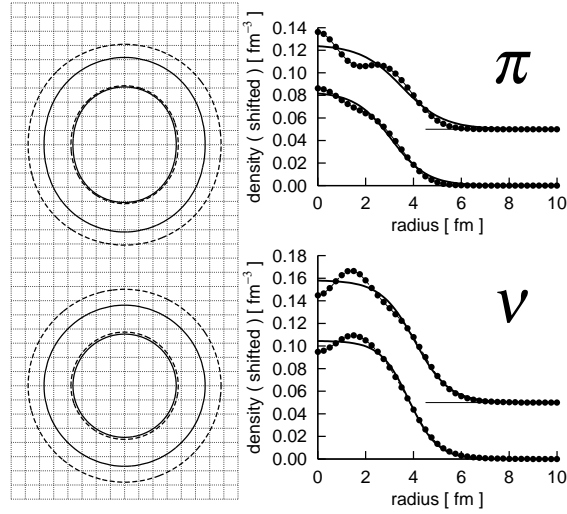


Figure 8. Neutron and proton density distributions in the ground state of  $^{50}\text{S}$ , calculated by the unrestricted SHF with SLy4 and with a mesh size of 0.25 fm. Left-hand side: equi-density lines with 50% and 1% of the central density in the  $(x, z)$  and  $(x, y)$  planes are drawn. Solid and dashed lines indicate those for protons and neutrons, respectively. Right-hand side: Density distributions along the major and minor axes are drawn by thin-solid lines with filled circles. The least-square fits of them with the Wood-Saxon function are also shown by solid lines. The former densities are shifted up by  $0.05 \text{ fm}^{-3}$  to facilitate the comparison.

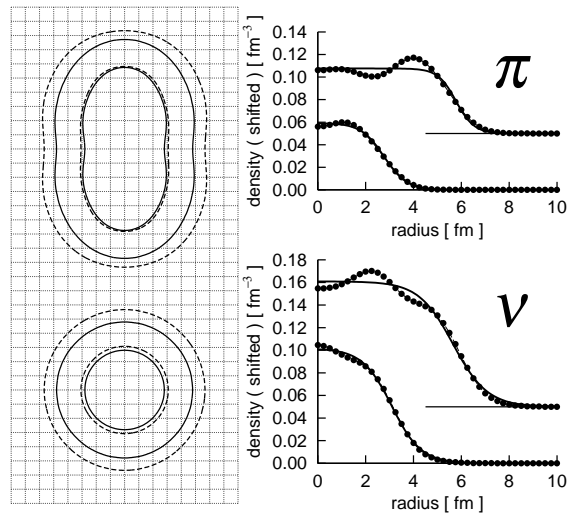


Figure 9. The same as Fig. 8 but for the SD state.

#### 4. Summary

With the use of the symmetry-unrestricted cranked SHF method in the 3D coordinate-mesh representation, we have carried out a systematic theoretical search for the SD and HD rotational bands in the  $N=Z$  nuclei from  $^{32}\text{S}$  to  $^{48}\text{Cr}$ . We have found the SD solutions in  $^{32}\text{S}$ ,  $^{36}\text{Ar}$ ,  $^{40}\text{Ca}$ ,  $^{44}\text{Ti}$ , and the HD solutions in  $^{36}\text{Ar}$ ,  $^{40}\text{Ca}$ ,  $^{44}\text{Ti}$ ,  $^{48}\text{Cr}$ . Particular attention has been paid to the recently discovered SD band in  $^{40}\text{Ca}$ , and we have found that the SD band in  $^{40}\text{Ca}$  is extremely soft against both the axially symmetric ( $Y_{30}$ ) and asymmetric ( $Y_{31}$ ) octupole deformations. Thus, it will be especially interesting to search for negative-parity rotational bands associated with non-axial  $K^\pi = 1^-$  octupole vibrations built on the SD yrast band.

We have also discussed possible presence of SD states in sulfur isotopes from  $^{46}\text{S}$  to  $^{52}\text{S}$ , which are situated near the neutron drip line. An interesting subject in this region is the appearance of deformed neutron skins both in the ground and SD states. The presence of the deformed neutron skins may be detected through excitation spectra of these nuclei. Thus, search for new kinds of soft  $K^\pi = 0^-$  and  $1^-$  (dipole + octupole) vibrational modes of excitation is challenging, both theoretically and experimentally.

#### References

1. C.E. Svenson *et al.*, Phys. Rev. Lett. 85 (2000) 2693.
2. E. Ideguchi *et al.*, Phys. Rev. Lett. 87 (2001), 222501.
3. C.D. O'Leary, M.A. Bentley, B.A. Brown, D.E. Appelbe, R.A. Bark, D.M. Cullen, S. Ertürk, A. Maj and A.C. Merchant, Phys. Rev. C 61 (2000) 064314.
4. M. Yamagami and K. Matsuyanagi, Nucl. Phys. A 672 (2000) 123.
5. M. Yamagami, K. Matsuyanagi and M. Matsuo, Nucl. Phys. A 693 (2001) 579.
6. T. Inakura, S. Mizutori, M. Yamagami and K. Matsuyanagi, Nucl. Phys. A 710 (2002) 261.
7. P. Bonche, H. Flocard, P.H. Heenen, Nucl. Phys. A 467 (1987) 115.
8. H. Imagawa and Y. Hashimoto, private communications.
9. T. Marumori, T. Maskawa, F. Sakata and A. Kuriyama, Prog. Theor. Phys. 64 (1980) 1294.